Charge and current sensitive preamplifier and pulse shape discrimination application*

Jishao Xu,[1,2] Xiguang Cao,[3,1,2,†] Ping Su,[4] Yibo Hao,[3,5] Gaoyi Cheng,[4] Zhengli Liao,[6] Weifu Yin,[1,2]
Yonghao Jin,[1,2] XiaoBao Wei,[5,7] Zengxiang Wang,[5,7] Guoqiang Zhang,[1,2] Ge Ren,[3,5] Tianren Zhuo,[5]
Yancheng Liu,[1,2] Yanyun Yang,[7] Junbing Ma,[7] Shiwei Xu,[7] Kang Wang,[7] Zhen Bai,[7] Guo Yang,[7]
Linghao Wang,[7] Yusen Wang,[8] Wanbing He,[4] Jiansong Wang,[8] Chunwang Ma,[9,5] and Deqing Fang[4]

[1] *Shanghai Institute of Applied Physics, Chinese Academy of Sciences, Shanghai 201800, China*
[2] *University of Chinese Academy of Sciences, Beijing 100049, China*
[3] *Shanghai Advanced Research Institute, Chinese Academy of Sciences, Shanghai 201210, China*
[4] *Key Laboratory of Nuclear Physics and Ion-Beam Application (MOE),*
Institute of Modern Physics, Fudan University, Shanghai 200433, China
[5] *College of Physics, Henan Normal University, Xinxiang 453007, China*
[6] *Center for instrumental analysis, Guangxi University, Nanning 530004, China*
[7] *Institute of Modern Physics, Chinese Academy of Sciences, Lanzhou 730000, China*
[8] *Huzhou University, Huzhou 313000, china*
[9] *Institute of Nuclear Science and Technology, Henan Academy of Science, Zhengzhou 450046, China*

In this study, a compact 16-channel integrated charge and current sensitive preamplifier, called CCPA, was developed for the large-scale detector array used in nuclear physics experiments. The CCPA is designed to achieve the pulse shape discrimination method for silicon detectors. The CCPA has a fast response of typically less than 6 ns for the pulse rise time and a low equivalent noise of 1.5 keV at zero input capacitance. Energy dynamic range and pulse decay time can be easily adjusted for different applications by changing the feedback capacitance C_f and resistance R_f. A good energy resolution of 26.87 keV was achieved for 5.486 MeV α particles from ^{241}Am. The pulse shape discrimination method was applied for the first time in the experiment carried out on the Radioactive Ion Beam Line in Lanzhou (RIBBL1), and the CCPA demonstrated high resolution and stability in beam experiments. The experiment has realized the identification of low energy α particles as low as 5 MeV by pulse shape discrimination method, as well as the hundreds MeV charged particle. It provides a new routine for high precision measurement of low energy charged particles emitted by light nuclear reactions.

Keywords: Exotic nuclear structures · Charge and current sensitive preamplifier · Pulse shape discrimination · Low energy charge particle · Silicon detector

I. INTRODUCTION

Clustering is prevalent in the ground states of light nuclei region far from the beta stability line, as well as in the excited states of nuclei along the stability line[1–5]. The cluster structure is of profound significance for understanding and validating various nuclear structure models, and it also plays a crucial role in the study of 3α reaction rates and the formation of P nuclei under high-temperature nuclear astrophysical conditions. When atomic nuclei are excited to high-energy and high-angular momentum states, they can exhibit various exotic shapes such as rings, cylinders, and bubble structures. There is a long history of theoretical studies on the possible existence of extremely exotic nuclear shapes. Wheeler proposed that under certain conditions, atomic nuclei can take on toroidal shapes. Following this suggestion, C.Y. Wong explored possible toroidal and bubble nuclei [6], predicting ring-like states in the mass regions of $40 \leq A \leq 70$ [7–9] and $A \leq 250$ [10, 11]. Theoretical studies suggest that these ring-like shapes arise from the interaction among nuclear, centrifugal and Coulomb forces. In the recent observation of the 7α decay of ^{28}Si, highly energetic resonant excited states were discovered, which are in good agreement with the theoretical predictions for excited toroidal ^{28}Si [12–15].

Similarly, Hoyle states have important implications for nuclear reactions and nucleosynthesis processes taking place in stellar environments. The Hoyle state of ^{12}C has been a notable example with well developed α cluster [16]. Recently, new evidence has been discovered for predicted possible Hoyle-like structures in ^{16}O[17]. Similarly, various α cluster structures have also been found in the $\alpha + ^2n + ^2n$ cluster structure of ^{8}He [18]. Other cluster structures have also been identified in ^{12}Be, ^{16}C, and ^{24}Mg [19–21]. These excited states of cluster nuclei and toroidal nuclei may possess exotic shapes and have the potential to decay into multiple α clusters. Experimental studies of nuclei with multiple α cluster states require precise and track coincidence measurements of the α particles emitted during the decay process. In order to study the exotic nuclear clustering structures mentioned above, we have developed a sophisticated telescope array [22].

The telescopes consist of two layers of DSSDs and CsI array to study of exotic nuclear clustering structures, detailed configurations can be found in the reference [22]. We use pulse shape discrimination (PSD) to identify charged particles to improve the performance of the detector array. The theoretical basis of pulse shape discrimination has been pro-

posed [23–25]. Large-scale charge particle arrays such as FAZIA [26–29], GRIT [30] have explored the technique of pulse shape discrimination in light and low energy particles, and have yet to be applied on a large scale to more general situations. Other large-scale arrays such as GODDESS [31], GASPARD [32], TRACE [33], and HYDE [34] under construction also plan to use this new method. The pulse shape discrimination method will be a new method with great potential and promise to greatly enhance the measurement capability of charged particles.

Charged particles emission manifest a rich physics near the cluster emission threshold. Recently, the photonuclear reaction performed on the HIγS facility has shown that the photonuclear reaction can be used as a new approach to study exotic nuclear clustering structures [36]. The intermediate energy gamma source in China, Shanghai Laser Electron Gamma Source (SLEGS), has been commissioned (Fig. 1) [37]. A new high-performance laser gamma source VEGA, is under construction at the ELI-NP nuclear facility [39]. The PSD method can serve as a powerful method to measure and identify the low energy charged particles emitted from photonuclear reaction [38]. Measurements of the ^{7}Li (γ, t) ^{4}He ground state cross section between $\boldsymbol{E}_\gamma = 4.4 \sim 10$ MeV have been performed at the HIγS facility of the TUNL, where an analysis of charged particles was performed using kinematic identification techniques [40]. Events matching $\alpha - t$ were severely affected by the electron background induced by the γ beam. Given that the mass of an electron is 935 times less than that of a proton, the pulse shape method is feasible to eliminate electronic background. Subsequently, kinematic discrimination can be used to extract the desired target events [41].

The preamplifier plays a pivotal role as an electronic module, serving to match the impedance between the detector and the spectroscopy amplifier. The Mesytec MPR-16 module [42], due to its big size, does not fit easily into large scale detector array. ORTEC charge-sensitive preamplifier modules 142A, 142B, and 142C [43] are designed with low noise and fast rise time, specifically tailored for optimal matching with single charged particle detector. The China Institute of Atomic Energy has successfully developed an integrated charge-sensitive preamplifier with good performance and stability in experiments [44]. However, the preamplifiers mentioned above are not designed for pulse shape discrimination and do not provide a separate current signal, which would allow a deeper investigation of PSD than the existing rise time signal analysis method using charge sensitive preamplifiers [28, 30, 45].

To facilitate a more comprehensive investigation into the field of pulse shape discrimination (PSD), H. Hamritas conceptualized a specialized charge and current sensitive preamplifier for pulse shape discrimination techniques utilizing silicon detectors [45]. This innovation was successfully employed in projects such as FAZIA. GRIT designed the iPACI chip specifically for PSD, capable of simultaneously outputting current and charge signals, reducing the amplifier size [30]. We have designed a 16-channel integrated Charge and Current sensitive Preamplifier (CCPA). The CCPA circuit fea-

tures a simple structure and low cost, enabling the widespread use of large-scale detector arrays. This advancement can drive the popularization of pulse shape discrimination (PSD) with silicon detectors. The CCPA, owing to its compact size, can be effectively cooled by a small water-cooled plate and can be easily placed in the vacuum target chamber for close connection with the silicon detector, thereby significantly reducing the noise level.

II. THE CIRCUIT DESIGN OF CCPA

The circuit of CCPA is divided into two key parts and its attached high voltage circuit for the detector, and test circuit. The two core components consist of an integrator circuit composed of C_1, R_1, and PA$_1$, and a differentiator circuit composed of C_2, C_3, R_3, and PA$_2$ (Fig. 2). The integrator circuit consists of a capacitor (C_1), a resistor (R_1), and an operational amplifier PA$_1$. The operational amplifier PA$_1$ in use is the low-noise 1.05 GHz FastFET operational amplifier. These amplifiers were developed with the Analog Devices, Inc., proprietary eXtra fast complementary bipolar (XFCB) process, which allows the amplifiers to achieve ultralow noise (4 nV/$\sqrt{\text{Hz}}$; 2.5 fA/$\sqrt{\text{Hz}}$) as well as very high input impedance. The resistance-capacitance feedback network, denoted as R_f, C_f, constitutes a charge integration and discharge circuit. The energy sensitivity and pulse decay time are determined by R_f, C_f and PA$_1$. PA$_2$ in conjunction with components C_2, C_3, and R_3 constitute the differential amplification circuit to provide the current signal from the silicon detector (Fig. 2). The PA$_2$ is a unity-gain stable, high speed, voltage feedback amplifier with low distortion, low noise, and high slew rate. The PA$_2$ has a bandwidth of 850 MHz, a slew rate of 2800 V/μs, and a ± 5 V supply voltage. It is an ideal candidate for systems that require high dynamic range, precision, and speed. The high-voltage circuit is comprised of two resistors, R_4, and a filtering capacitor, C_4, aimed at eliminating minor high-frequency noise from the high-voltage power supply.

CCPA's PCB has 6 layers, including the signal layer, the ground layer, the positive power layer, the ground layer, the negative power layer, and the ground layer (Fig. 3). A high impedance node is susceptible to picking up stray signals in the system, so keeping it as short as possible reduces this effect. The layout of an input node with a high impedance is of great importance. Other signals should be located away from this signal path and there should be no internal power planes underneath it, where space is limited, we slot around high impedance input nodes to provide additional isolation and reduce the effects of contamination. The signal layer and the ground layer establish an approximate 50-ohm impedance. The output signal employs an MCX interface to connect coaxial cables for data acquisition to reduce signal interference while preserving a compact form factor. All signal interfaces are installed on the rear side to facilitate direct contact between the front chip and the water cooler for heat dissipation. The system is cooled by a liquid cooling radiator, which can cool the CCPA to room temperature while the CCPA works
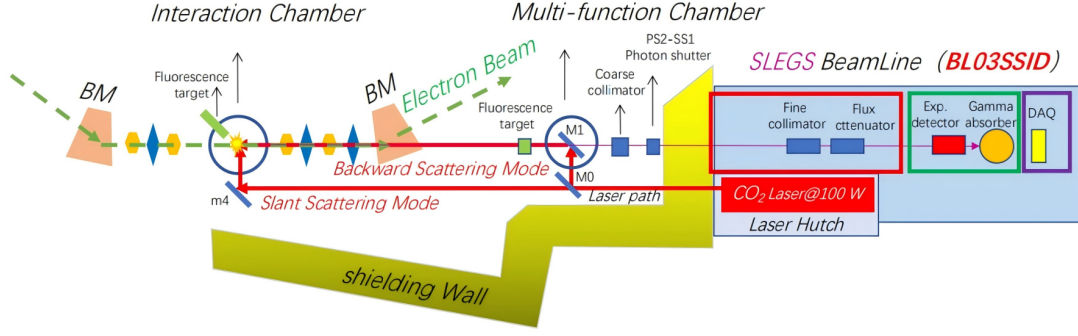
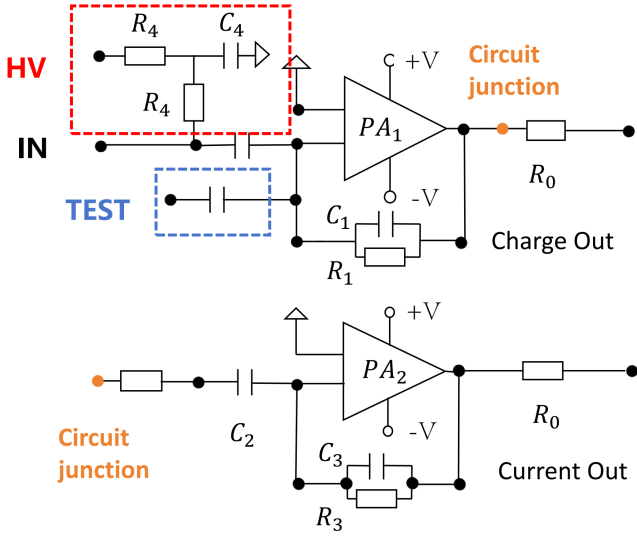Fig. 1. Schematic layout of the SLEGS beamline from literature [37]
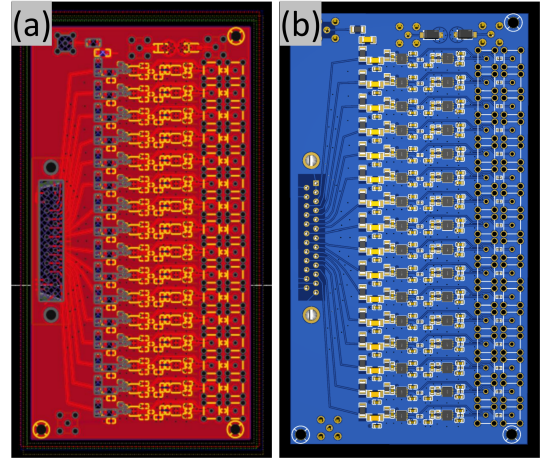

Fig. 2. CCPA circuit schematic

Fig. 3. The circuit board design of the CCPA (a) and architecture diagram with capacitors, resistors, and operational amplifiers (b).

at full power in a vacuum.

III. PERFORMANCE TEST RESULTS

We conducted a comprehensive test of the CCPA using a pulse generator and an α source to gain a clearer understanding of the preamplifier's performance. CCPA shows good performance in linearity, speed, and resolution tests.

A. Linearity test

Linearity is very important for spectrum measurement. We conducted linearity testing on the CCPA using the DG5352 function generator produced by RIGOL. We generated ramps using the DG5352, and injected the signal into the amplifier, and observed that the current waveform yielded a pulse width of 25 ns.

We employed a Tektronix oscilloscope to observe the waveforms of the current and charge signals. The signals were then routed to a DT5730 digitizer for digital processing.

Charge and current amplitude values are shown (Fig. 4) as a function of the input energy, expressed in MeV and μA. linear fitting is applied to the data points, and the linearity of both the charge signal and the current signal is excellent with the $R^2 = 0.99996$ for the charge signal, and the $R^2 = 0.99997$ for the current signal. This shows that CCPA has good linearity.

B. Speed test

We utilized the DG5352 function generator produced by RIGOL for speed measurements on CCPA.We used the DG5352 to generate fast rising signals (with a rise time $(10\% - 90\%)$ of 2.9 ns). and input signals to CCPA with a 30 cm coaxial cable. By adjusting this signal, the CCPA can output at full scale. The measured rise time for the charge signal of CCPA was 8.7 ns, and for the current signal, it was 5 ns. Removed the rising edge time of the function generator itself, we obtained a response time for CCPA of less than 6 ns (0 pF).
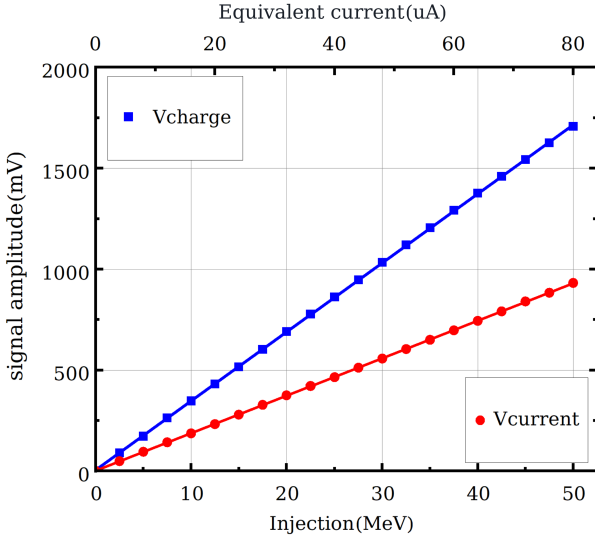
Fig. 4. Linearity plot.

C. α sources test and energy resolution

We connected a CCPA ($C_1 = 1$ pF) to a 300 μm W1 type Double-Sided Silicon Strip Detector (DSSD) manufactured by Micron Semiconductor Ltd. Company. ^{241}Am α source was used to evaluate the energy resolution. The signal generated by the CCPA is fed into the oscilloscope, as shown in Figure 5a, which not only clearly displays the charge signal, but also the current signal. The noise of charge signal and current signal is less than 2 mV and 1 mV, respectively. Then the generated signal was input into the CAEN DT5730 digitalizer. We employed a trapezoidal filter to filter and shape the charge signal. The obtained α source ene spectrum is shown in the Fig. 5b below. The energy resolution can reach 0.49%. The equivalent charge noise is 26.87 keV. Generating a signal with the same amplitude using a function generator, the resolution is 0.1%. The equivalent charge noise (0 pF) of the CCPA is 5.4 keV.

Prior to beam experiments, we also tested the PSD of the CCPA ($C_1 = 5$ pF) with a 300 μm DSSD using three α sources. The PSD particle identification spectrum shown in Fig. 5c clearly reveals the presence of α particles with three energies. The PSD method we used in Fig. 5c was "Energy vs Current maximum" method. CCPA can reach very high resolution due to its low noise. α particles of different energies form a band in the diagram.

IV. IN BEAM EXPERIMENT OF THE CCPA

The CCPA modules were applied to a beam experiment at the Radioactive Ion Beam Line in Lanzhou (RIBLL1), with a 35 MeV/u ^{28}Si beam incident on a 1 mg/cm^2 ^{27}Al target. To study the 7α disassembly of ^{28}Si, we utilized six sets of telescopes to detect charged emitted particles. Fig. 6 shows the layout detector array used for the experiment. 1# telescope ,
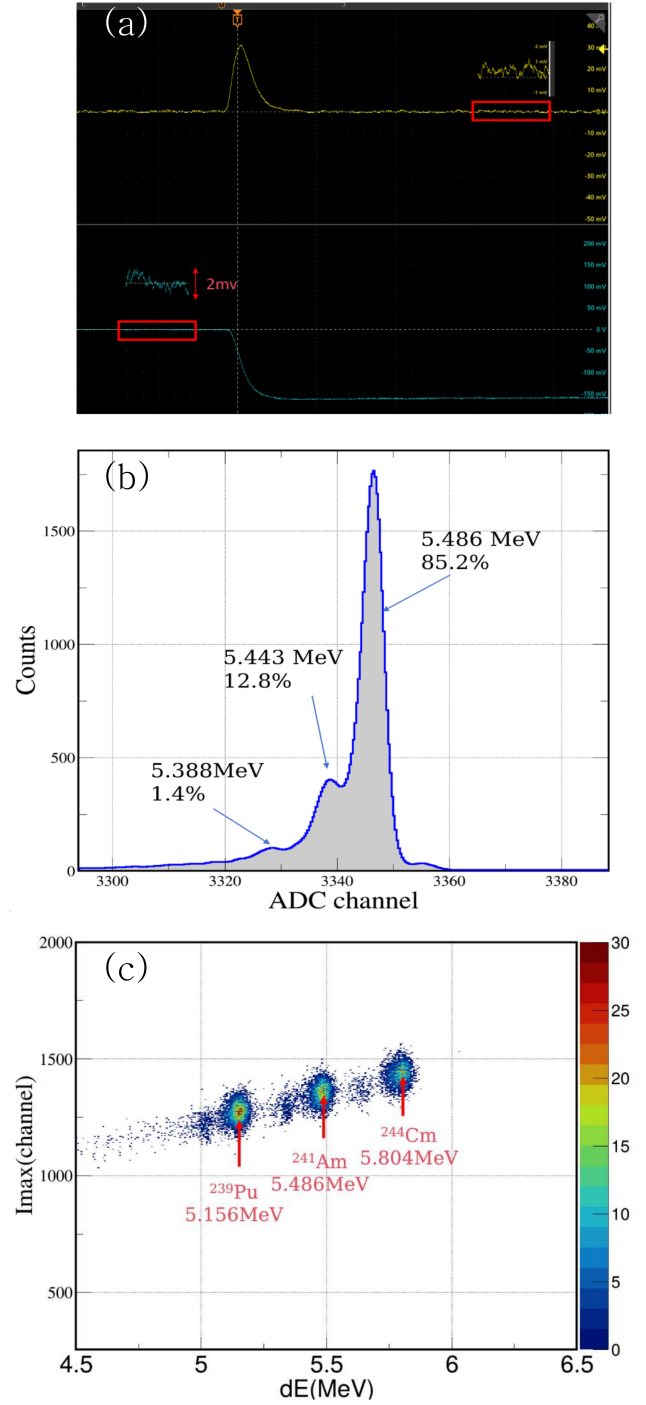

Fig. 5. (a).The plot shows the charge signal (blue), the current signal(yellow) and their associated noises, measured with an α source. (b) .^{241}Am α energy spectra measured by the DSSD with CCPA.(c). Particle Identification Diagram Using Pulse Shape Discrimination Method for Measuring Three-Component α Sources, the Energy value is plotted as the x-axis, and the maximum amplitude of the current pulse signal is plotted as the y-axis.

Fig. 6. The photograph of the telescope array used in the experiment, showing the spatial layout of the individual telescopes.
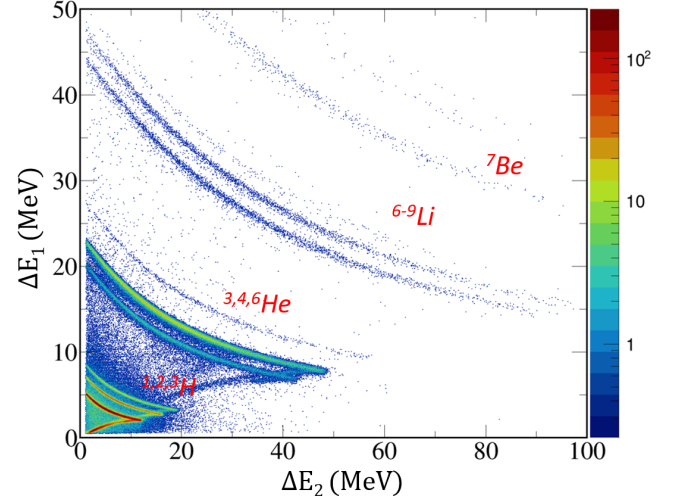

Fig. 7. $\Delta E - E$ correlation for 5# telescope , using a 300 μm silicon detector (Si_1) and a 1000 μm silicon detector (Si_2): the x-axis gives the energy deposited in Si_2, the y-axis that in Si_1.

2# telescope , and 3# Telescope are composed of a 300 μm and a 1000 μm BB7-type DSSD, along with a 3x3 CsI-PMT array. 4# telescope is comprised of a 300 μm and a 500 μm BB7-type DSSD, along with a 3x3 CsI-PMT array. 1#, 2#, 3#, and 4# telescope are positioned symmetrically around the beam axis. 5# telescope and 6# telescope each utilize a configuration consisting of a 300 μm and a 1000 μm W1-type DSSD, along with a 5x5 CsI-SiPM array.

DSSDs of telescope comprises that are coupled to the CCPA, with the CsI-SiPM utilizing a custom-designed current preamplifier for signal shaping before output. The CCPA is situated within a vacuum chamber located in close proximity to the DSSD. In this experiment, for the 300 μm silicon detector, we employed a 5 pF feedback capacitance for CCPA, which can be capable of handling an energy range exceeding 400 MeV. For the 1000 μm silicon detector, a CCPA preamplifier with a feedback capacitance of 12 pF was used, suitable for an energy range greater than 900 MeV.

We employed the MDPP-32 digitizer manufactured by Mesytec company to acquire the preamplifier signals. The digitizer is placed outside the vacuum chamber and connected to the CCPA using a coaxial cable through a flange. The digitizer is mounted in the air and connected to CCPA via coaxial cables. By adjusting the gain of the digitizer, we optimized the energy dynamic range to achieve the best discrimination of the emitted particles.

A. Identification of fragments with ΔE (Si_1) $- E$ (Si_2) method

The $\Delta E - E$ technique is based on the Bethe-Bloch energy loss formula by measuring the particle energies deposited by the particle in two detectors after passing through the first layer. In the $\Delta E - E$ correlation, a particle stopped in Si_2 helps to work out one of the quasi-hyperbolic correlations often used to identify particles: as the energy of the incident particle E_0 increases, the energy of Si_1 decreases and that of Si_2 increases. As E_0 increases, Si_2 can not stop the particles, then the energy deposited in Si_1 and Si_2 decreases[41, 47, 49].

The detector array equipped with CCPA preamplifiers demonstrated excellent performance through the in beam experiment. The energy resolution of the detector system consistently kept better than 1% in beam experiment. Fig. 7 illustrates a typical ΔE (Si_1) $- E$ (Si_2) particle identification plot of 5# telescope . We can observe that throughout the entire dynamic range, all detected elements are clearly identifiable. The isotope bands are distinct and well-separated.

A Figure of Merit (FoM) is defined as

$$FoM = \frac{|\overline{PID_2} - \overline{PID_1}|}{FWHM_1 + FWHM_2} \quad (1)$$

was determined for adjacent A as a function of the energy. Here $FWHM_1$, $FWHM_2$ are the full widths at half maximum of the Gaussian distributions of two adjacent isotopes of atomic number A, $A+1$, and where $\overline{PID_1}$ and $\overline{PID_2}$ are the centroids of the peaks. We straightened and projected the isotope bands using CERN ROOT, as shown in Fig. 8. If FoM is greater than 0.7, the isotope bands are considered "well separated" [29, 45]. For the helium-3 and helium-4 isotope bands in Fig. 8, FoM is equal to 2.35. It means that very good identification is obtained. As well as in Fig. 7, the well can be observed. We optimized the energy dynamic range to achieve the best discrimination of the emitted particles. All telescope arrays in the report exhibit similar performance characteristics. This demonstrates that our CCPA preamplifier possesses a high energy resolution and identification ability in beam experiments.

B. Particle Identification with $\Delta E(Si_1 + Si_2) - E$ (CsI(Tl)) method

The most energetic particles pass through both silicon detectors and reach the following CsI(Tl) scintillators [41].

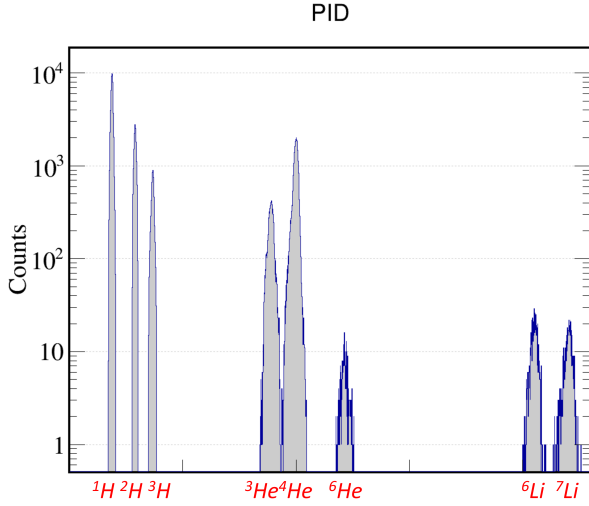Fig. 8. Particle identification (PID) spectrum obtained for 5# telescope with the $\Delta E(\mathrm{Si_1}) - E(\mathrm{Si_2})$ method.
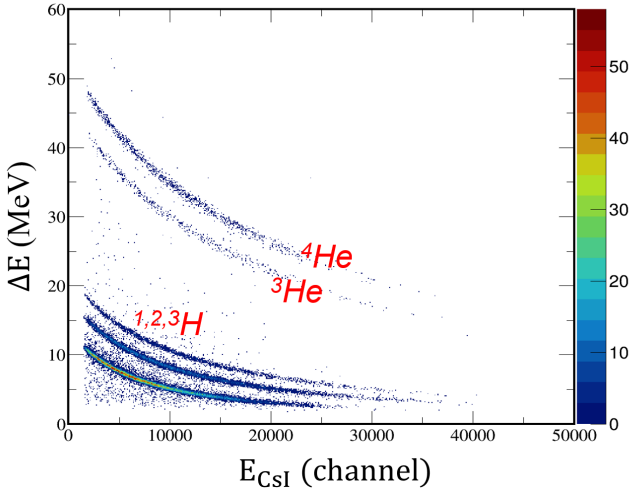

Fig. 9. Particle identification (PID) spectrum obtained for telescope 5 with the $\Delta E(\mathrm{Si_1 + Si_2}) - E(\mathrm{CsI})$ method.

Here the x-axis gives the light output of the CsI (Tl) scintillators collected by Sipm and the y-axis gives the total energy measured by the two silicon detectors (Fig. 9). We can clearly separate the isotopes of hydrogen and helium. The heavier elements, on the other hand, are stopped in the silicon detector because of poor penetration. This further demonstrates the high energy resolution and discrimination ability of our CCPA in beam experiments. Detailed information about CsI-SiPM arrays and their specific performance will be covered in a separate paper.

C. Light particles Identification with Pulse shape discrimination method

The PSD method uses the dependence of the pulse shape of the detector signal on the Z and A of the incident particle to extract information about the particle type [48]. The PSD method has been widely used in scintillator detectors and its application to silicon detectors has become a focus of research in recent years. This method allows particle identification using only the energy and signal rise time information of a single silicon detector, which not only greatly reduces the threshold for particle identification, but also reduces the complexity of the detector. PSD requires a detector energy measurement the energy of the stopped reaction product and an additional parameter related to the charge collection, i.e. the shape of the charge or current signal. In this study, the shape dependent parameter we used is the maximum value of the current signal versus energy.

The ΔE-E method employs two detectors to separately measure the particle ΔE deposited in the first detector and the residual E in the following detector. Particle identification is achieved based on the different deposited energies dependent on different types of particles in the ΔE and E silicon detectors. The particle identification threshold of the ΔE-E method depends on the thickness of the ΔE detector [24]. By using a thinner ΔE detector, the PID threshold can be further reduced. For instance, to pass through a 60 μm DSSD requires at least 9.2 MeV of particle energy, which means the minimum energy for identifying α and is more than 9.2 MeV by the ΔE-E method. In realistic measurements, a smaller threshold value is required. Due to manufacturing process limitations, thinner silicon detectors have poorer thickness uniformity. The aforementioned 60 μm silicon detector has a thickness non-uniformity larger than 4%, resulting in a poor energy measurement accuracy that does not meet experimental requirements [48].

Research indicates that compared to front-side incidence, rear side incidence, particles entering from the side with lower electric field strength, are more favorable for extracting particle species information from the pulse shape [41, 46]. This is attributed to the fact that under rear side incidence conditions, the plasma effect broadens the variation range of the signal rise time in silicon detectors. In order to better study pulse shape discrimination, DSSDs of 5# and 6# telescopes are positioned to face the beam with rear side, so that the products emitted from the reactions are injected into the DSSDs from the rear side. Simultaneously, we employed the PADC mode of the MDPP-32 digitizer to acquire the peak values of the current pulses. In this way, it is possible to maximize the rise-time differences of the charge signals produced by different stopped products with the same energy.

We draw a two-dimensional spectrum of the maximum value of the current signal pulse and the energy signal. We can clearly distinguish the α band shown in Fig. 10. Particles of different charges are clearly distinguished, forming a parabola-like band. Particles with large charges require high energy to penetrate the same thickness of silicon, and at the same time, particles with large charges of
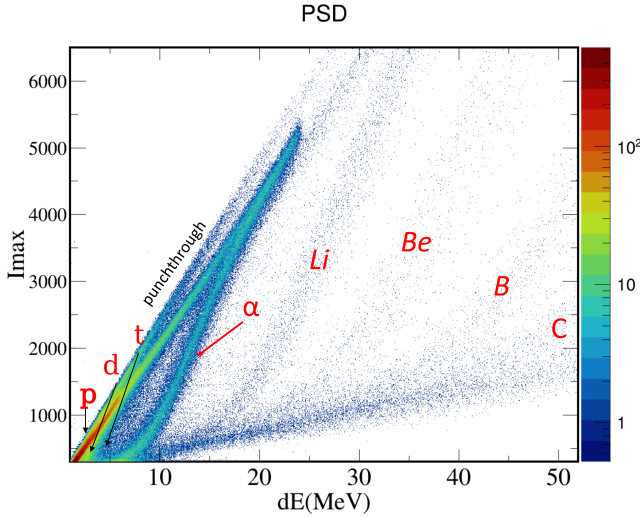
Fig. 10. Correlation "Energy vs Charge rise-time" for nuclei stopped in the 300 μm silicon detector .

the same energy form plasma columns in silicon detectors that dissociate slowly, resulting in a small current signal and a high discrimination threshold. The information presented in Fig. 10 is consistent with this physical rule. The pulse shape discrimination method compensates for the drawback of the $\Delta E(\mathrm{Si}_1) - E(\mathrm{Si}_2)$ method, which is unable to distinguish low-energy particles stopped in the first layer silicon. This enables us to identify 5 MeV α particles. If using the $\Delta E(\mathrm{Si}_1) - E(\mathrm{Si}_2)$ method, it is necessary to use silicon detectors thinner than 60 μm to achieve the discrimination of charged particles at such low energies. However, due to the junction capacitance of silicon detectors and manufacturing limitations, the energy resolution of thin silicon strips (< 60 μm) is significantly inferior to that of 300 μm silicon detectors.

It should be noted that many factors influence the effectiveness of pulse shape discrimination. The sampling frequency of the digitizer plays a critical role in accurately capturing current signal information. It has been shown that sampling rates below 200 MSa/s significantly degrade the quality of the discrimination [51]. In this experiment, the PADC of the MDPP32 (80 MHz) lacks adequate filtering functionality for fast pulses less than 100 ns. The application of appropriate filtering algorithms can reduce reliance on high sampling rates and enhance discrimination ability [27, 51]. For the discrimination of light particles from low energy nuclear reactions, the choice of a high gain version of the preamplifier can improve the discrimination quality. Similarly, the use of high-quality silicon detectors is essential [29, 53]. Currently, the pulse shape method using silicon detectors allows the identification of light particles (Z=1) with energies as low as 2 MeV [41, 52, 54].

V. SUMMARY

We have developed a new type of preamplifier CCPA,a 16-channel, fast-responding and high-resolution charge and current output preamplifier, and applied it on a large scale in beam experiment. The good performance of CCPA was further confirmed using an α source test.Silicon-silicon-CsI(TI) detectors have been used in an experiment setup, with a beam of 35 MeV/u ^{28}Si incident on ^{27}Al targets in order to investigate nuclear exotic configuration α-clusters. The detector array used in this experiment has been demonstrated to possess high energy resolution, high granularity, and strong identification ability. The results of the digital Pulse Shape discrimination technique for identifying stopped reaction products are highly satisfactory. The products with different Z can be clearly separated. If a CCPA with a higher gain is employed and the filtering capability of the digitizer is enhanced, the PSD method will yield better results. This study provides a new routine for the realization of high energy resolution and strong particle identification of products from in low-energy nuclear physics such as photonuclear reactions.

[1] Y.G. Ma, Effects of α-clustering structure on nuclear reaction and relativistic heavy-ion collisions. Nuclear Techniques. **8**, 46 (2023). https://10.11889/j.0253-3219.2023.hjs.46.080001

[2] W.B. He, Y.G. Ma, X.G. Cao et al., Giant Dipole Resonance as a Fingerprint of α Clustering Configurations in ^{12}C and ^{16}O. Phys. Rev. Lett. **113** 113, 032506 (2014). https://doi.org/10.1103/PhysRevLett.113.032506.

[3] B. Dey, S.S. Wang, D. Pandit et al., Exotic nuclear shape due to cluster formation at high angular momentum. Phys. Rev. C **102** , 031301 (2020). https://doi.org/10.1103/PhysRevC.102.031301.

[4] S.S. Wang, Y.G. Ma, W.B. He et al., Influences of α-clustering configurations on the giant dipole resonance in hot compound systems. Phys. Rev. C **108**, 014609 (2023). https://doi.org/10.1103/PhysRevC.108.014609.

[5] K. Wei, Y.L. Ye, Z.H. Yang, Clustering in nuclei: progress and perspectives. Nucl. Sci. Tech. **35**, 216 (2024). https://doi.org/10.1007/s41365-024-01588-x.

[6] G. Ren, C.W. Ma, X.G. Cao, et al. Bubble 36Ar and its new breathing modes. Phys. Lett. B **857**, 138990 (2024). https://doi.org/10.1016/j.physletb.2024.138990.

[7] A.Kosior, A.Staszczak, C.Y. Wong, Toroidal Nuclear Matter Distributions of Superheavy Nuclei from Constrained Skyrme-HFB Calculations, Acta Physica Polonica B, Proceedings Supplement, Vol. 10, pp. 249–258 (2017). http://dx.doi.org/10.5506/APhysPolBSupp.10.249

[8] C.Y. Wong, Toroidal nuclei. Phys. Lett. B. **41**, 446 (1972). https://doi.org/10.1016/0370-2693(72)90671-5.

[9] C.Y. Wong, Toroidal and spherical bubble nuclei. Ann. Phys. **77**, 279 (1973). https://doi.org/10.1016/0003-4916(73)90420-X.

[10] C.Y. Wong, Rotating toroidal nuclei. Phys. Rev. C. **17**, 331 (1978). https://doi.org/10.1103/PhysRevC.17.331.

[11] C.Y. Wong, Hot Toroidal and Bubble Nuclei. Phys. Rev. Lett. **55**, 1973 (1985). https://doi.org/10.1103/PhysRevLett.55.1973.

[12] X.G. Cao, E. Kim, K. Schmidt. et al., Examination of evidence for resonances at high excitation energy in the 7α disassembly of Si28. Phys. Rev. C. **99**, 014606 (2019). https://doi.org/10.1103/PhysRevC.99.014606.

[13] X.G. Cao, E.J. Kim, K. Schmidt, et al., α and α Conjugate Fragment Decay from the Disassembly of ^{28}Si at Very High Excitation Energy. JPS Conf. Proc. **32**, 010038 (2021). https://doi.org/10.7566/JPSCP.32.010038.

[14] X.G. Cao, E.J. Kim, K. Schmidt et al., Evidence for resonances in the 7α disassembly of ^{28}Si. AIP. Conf. Proc. **2038**, 020021 (2018). https://doi.org/10.1063/1.5078840.

[15] Z.X. Ren, P.W. Zhao, S.Q. Zhang et al., Toroidal states in ^{28}Si with covariant density functional theory in 3D lattice space. Nucl. Phys. A **996**, 121696 (2020). https://doi.org/10.1016/j.nuclphysa.2020.121696.

[16] M. Chernykh, H. Feldmeier, T. Neff et al., Structure of the Hoyle State in ^{12}C. Phys. Rev. Lett. **98**, 032501 (2007). https://doi.org/10.1103/PhysRevLett.98.032501.

[17] J.H. Chen., Y.L. Ye., K. Ma et al., New evidence of the Hoyle-like structure in ^{16}O. Sci. Bull. **68**, 1119 (2023). https://doi.org/10.1016/j.scib.2023.04.031.

[18] Z.H. Yang , Y.L. Ye , B. Zhou et al., Observation of the Exotic 0_2^+ Cluster State in ^{8}He. Phys. Rev. Lett. **131**, 242501 (2023). https://doi.org/10.1103/PhysRevLett.131.242501.

[19] M. Freer, H. Horiuchi, Y. Kanada-En'yo et al., Microscopic clustering in light nuclei. Rev. Mod. Phys. **90**, 035004 (2018). https://doi.org/10.1103/RevModPhys.90.035004.

[20] Z.H. Yang, Y.L. Ye, Z.H. Li et al., Observation of Enhanced Monopole Strength and Clustering in ^{12}Be. Phys. Rev. Lett. **112**, 162501 (2014). https://doi.org/10.1103/PhysRevLett.112.162501.

[21] D.X. Wang, Y.L. Ye., C.J. Lin et al., α-cluster decay from ^{24}Mg resonances produced in the ^{12}C $(^{16}$O,^{24}Mg$)$ α reaction. Chin. Phys. C. **47**, 014001 (2023). https://doi.org/10.1088/1674-1137/ac9e9a.

[22] Z.L.Liao, X.G. Cao, Y.X. Yang, et al., Design and construction of charged-particle telescope array for study of exotic nuclear clustering structure. Nucl. Sci. Tech. **35**, 134 (2024). https://doi.org/10.1007/s41365-024-01503-4.

[23] C. Leroy, P.Roy, G.L. Casse, et al., Charge transport in non-irradiated and irradiated silicon detectors. Nucl. Instrum. Methods A. **434**, 90 (1999). https://doi.org/10.1016/S0168-9002(99)00437-4.

[24] N.Le Neindre, R. Bougault, S. Barlini, et al., Comparison of charged particle identification using pulse shape discrimination and $\Delta E - E$ methods between front and rear side injection in silicon detectors. Nucl. Instrum. Methods A. **701**, 145 (2013). https://doi.org/10.1016/j.nima.2012.11.005.

[25] M. Pârlog, H.Hamrita, B. Borderie et al., Description of current pulses induced by heavy ions in silicon detectors. Nucl. Instrum. Methods A. **613**, 290 (2010). https://doi.org/10.1016/j.nima.2009.12.010.

[26] S. Barlini,R. Bougault,Ph.Laborie, et al., New digital techniques applied to A and Z identification using pulse shape discrimination of silicon detector current signals. Nucl. Instrum. Methods Phys. Res. A. **600**, 644 (2009). https://doi.org/10.1016/j.nima.2008.12.200.

[27] J.A. Dueñas, D. Mengoni, V. Parkar, et al., Identification of light particles by means of pulse shape analysis with silicon detector at low energy. Nucl. Instrum. Methods A. **676**, 70 (2012). https://doi.org/10.1016/j.nima.2012.02.032.

[28] L. Bardelli, M. Bini, G. Casini, et al., Progresses in the pulse shape identification with silicon detectors within the FAZIA Collaboration. Nucl. Instrum. Methods A. **654**, 272 (2011). https://doi.org/10.1016/j.nima.2011.06.063.

[29] S. Carboni, S. Barlini, L. Bardelli et al., Particle identification using the $\Delta E - E$ technique and pulse shape discrimination with the silicon detectors of the FAZIA project. Nucl. Instrum. Methods A. **664**, 251-263 (2012). https://doi.org/10.1016/j.nima.2011.10.061.

[30] J.J. Dormard, M. Assié, L. Grassi et al., Pulse shape discrimination for GRIT: Beam test of a new integrated charge and current preamplifier coupled with high granularity Silicon detectors. Nucl. Instrum. Methods A. **1013**, 165641 (2021). https://doi.org/10.1016/j.nima.2021.165641.

[31] S.D. Pain, A. Ratkiewicz,T. Baugher, et al., Direct Reaction Measurements Using GODDESS. Phys. Procedia. **90** , 455-462 (2017). https://doi.org/10.1016/j.phpro.2017.09.051.

[32] GASPAED Project http://gaspard.in2p3.fr.

[33] TRACE Project http://spes.lnl.infn.it/ index.php/researchon-nuclear-physics/150-traceS.

[34] HYDE Project http://www.uhu.es/gem/proyectos/hydeS.

[35] S. Wuenschel, K. Hagel, L.W. May et al., Particle Identification in the NIMROD-ISiS Detector Array. AIP Conf. Proc. 1099, 1 (2009). https://doi.org/10.1063/1.3120164.

[36] W.R. Zimmerman, M.W. Ahmed, B. Bromberger et al., Unambiguous Identification of the Second 2^+ State in ^{12}C and the Structure of the Hoyle State. Phys. Rev. Lett. **110**, 152502 (2013). https://doi.org/10.1103/PhysRevLett.110.152502.

[37] L.X. Liu, H.W. Wang, G.T. Fan et al., The SLEGS beamline of SSRF. Nucl. Sci. Tech. **35**, 111 (2024). https://doi.org/10.1007/s41365-024-01469-3.

[38] Y.N. Gu, W.J. Zhao, X.G. Cao et al. Feasibility study of the photonuclear reaction cross section of medical radioisotopes using a laser Compton scattering gamma source. Nucl. Sci. Tech. **35**, 155 (2024). https://doi.org/10.1007/s41365-024-01481-7.

[39] O. Tesileanu, M. Gai, A. Anzalone, et al., Charged particle detection at ELI-NP. Rom. Rep. Phys. **68**, 699-734 (2016).

[40] M. Munch, C. Matei, S.D. Pain et al., Measurement of the ^{7}Li$(\gamma, t)^4$He ground-state cross section between $E_\gamma = 4.4$ and 10 MeV. Phys. Rev. C. **101** , 055801 (2020). https://doi.org/10.1103/PhysRevC.101.055801.

[41] B. Genolini, B. Le Crom, M. Assié et al., Pulse shape discrimination at low energies with a double sided, small-pitch strip silicon detector. Nucl. Instrum. Methods A. **732**, 87 (2013). https://doi.org/10.1016/j.nima.2013.06.078.

[42] Mesytec MPR-16-Series http://www.mesytec.com/products/data sheets/MPR-16.pdf.

[43] H. Hamrita, E. Rauly, Y. Blumenfeld et al., Charge and current-sensitive preamplifiers for pulse shape discrimination techniques with silicon detectors. Nucl. Instrum. Methods A. **531**, 607-615 (2004). https://doi.org/10.1016/j.nima.2004.05.112.

[44] D.X. Wang, C.J. Lin, L. Yang et al. Compact 16-channel integrated charge-sensitive preamplifier module for silicon strip detectors. NUCL. SCI. TECH **31**, 48 (2020). https://doi.org/10.1007/s41365-020-00755-0.

[45] G. Li, J.L. Lou, Y.L. Ye et al., Property investigation of the wedge-shaped CsI(Tl) crystals for a charged-particle telescope. Nucl. Instrum. Methods A.**1013**, 165637 (2021). https://doi.org/10.1016/j.nima.2021.165637.

[46] S. Barlini, S. Carboni, L.Bardelli et al., Effects of irradiation of energetic heavy ions on digital pulse shape analysis with silicon detectors. Nucl. Instrum. Methods A.**707**, 89-98 (2013). https://doi.org/10.1016/j.nima.2012.12.104.

[47] J. Ammerlaan, F. Rumphorst, Ch. Koerts et al., Particle identification by pulse shape discrimination in the p-i-n type semiconductor detector. Nucl. Instrum. Methods. **22**, 189-200 (1963). https://doi.org/10.1016/0029-554X(63)90248-9.

[48] P. Li, Z. Li, Z. Chen et al., Digital Pulse Shape Discrimination for Silicon Detector. Nucl. Phys. Rev. **34**, 177-183 (2017). https://doi.org/10.11804/NuclPhysRev.34.02.177.

[49] G.Y. Cheng, Q.M. Su, X.G. Cao et al. The study of intelligent algorithm in particle identification of heavy-ion collisions at low and intermediate energies. Nucl. Sci. Tech. **35**, 33 (2024). https://doi.org/10.1007/s41365-024-01388-3

[50] G.Y. Cheng, X.G. Cao, Q.M. Su et al. Research on charged particle identification of telescope in heavy-ion collisions at low and intermediate energies based on optimization algorithms. Nucl. Instrum. Methods B, **554**, 165453 (2024). https://doi.org/10.1016/j.nimb.2024.165453.

[51] M. Assié, B. Le Crom, B. Genolini, et al., Characterization of light particles ($Z \leq 2$) discrimination performances by pulse shape analysis techniques with high-granularity silicon detector. Eur. Phys. J. A. **51**, 11 (2015). https://doi.org/10.1140/epja/i2015-15011-6.

[52] K. Mahata, A. Shrivastava, J.A. Gore et al., Particle identification using digital pulse shape discrimination in a nTD silicon detector with a 1 GHz sampling digitizer. Nucl. Instrum. Methods A.**894**, 20-24 (2018). https://doi.org/10.1016/j.nima.2018.03.052.

[53] L. Bardelli, M. Bini, G. Casini, et al., Influence of crystal-orientation effects on pulse-shape-based identification of heavy-ions stopped in silicon detectors. Nucl. Instrum. Methods A. **605**, 353-358 (2009). https://doi.org/10.1016/j.nima.2009.03.247.

[54] M. Assié, A. Matta, B. Le Crom et al., New methods to identify low energy ^{3}He with Silicon-based detectors. Nucl. Instrum. Methods A.**908**, 250-255 (2018). https://doi.org/10.1016/j.nima.2018.08.050.